EXPERIMENTAL IMPLEMENTATION OF SDRE METHOD FOR AUTONOMOUS RENDEZVOUS AND DOCKING MANEUVERING

G. Di Mauro[(1)], **M.Schlotterer**[(2)], **S. Theil**[(2)] **and M. Lavagna** [(1)]
[(1)] Aerospace Engineering Department, Politecnico di Milano, Via La Masa 34, 20156 Milano, Italy
[(2)] DLR Institute of Space Systems, Robert-Hooke-Str.7, 28359 Bremen, Germany

Abstract: *In this paper a nonlinear controller technique, referred to State-Dependent Riccati Equation (SDRE), is exploited to handle relative position tracking and attitude synchronization problem involving in docking manoeuvring operations between two Earth orbiting satellites. More specifically a testbed developed by DLR-Institute of Space Systems is used for testing the proposed control algorithm. The experimental results show the effectiveness of SDRE controller for proximity operations problem and its feasibility for real-time implementation on the hardware.*

Keywords: *Nonlinear Control, R&D Maneuvering, R&D Testbed*

1. Introduction

Nowadays autonomous rendezvous and docking (AR&D) operations represent a crucial technique for several space missions which involve either in orbit assembly of numerous modules or serving/refueling operations; both around Earth and interplanetary scenarios, manned and unmanned vehicles may ask for such a technique.
The space programs history is studded with several examples of human supported R&D mission; anyhow, the autonomy in R&D manoeuvring is still an unresolved issue. The benefit of incremented autonomy for this kind of space applications is evident: manoeuvres can be performed timely far from Earth overcoming problems due to large communication delays; ground stations and control centres can lighten their load devolving on board recursive manoeuvres of Earth orbiting systems; the chance to exploit unmanned vehicles may reduce the failure risk due to human error. For these reasons the scientific community did many efforts to develop a completely autonomous system for R&D operations. To gain reliability, robustness and confidence in designing and implementing autonomous R&D systems significant on-ground and in orbit testing campaigns have been planned and partially accomplished within the last decade, focused on both software and hardware technology validation.
In this paper we summarize the efforts to settle an experimental facility to support the autonomous rendezvous and docking demonstrations and testing; more specifically, we use the developed testbed to demonstrate the feasibility of real-time execution of a nonlinear controller, named *State-Dependent Riccati Equation (SDRE)*, originally proposed by Pearson and then described in details by Cloutier, Hammett, Beeler and Çimen, [1], [2],[3], and[4]. By matching the Linear Quadratic Regulator (LQR), this method allows to compute a sub-optimal solution of nonlinear control problem by solving online an Algebraic Riccati Equation (ARE). Thus, it represents an effective

option to issues involved with solving nonlinear Hamilton-Jacobi-Bellman partial differential equations associated with nonlinear control problem; moreover, thanks to its formulation, it offers the same design flexibility of LQR, allowing to regulate the control signal magnitude by adjusting the entries in the penalty state-dependent matrices. On the other hand, it is sensitive to computational cost due to the online solution of an ARE, as illustrated in [5] where SDRE method has been exploited to solve both formation flying keeping and docking manoeuvring problems. This aspect represents the main drawback of the SDRE technique, which might demand significantly more computational resources than conventional control algorithms, especially for high-order systems control. For this reason the hardware implementation of SDRE approach was scarce and restricted to low-order systems: Erdem *et al.* exploited the SDRE technique to control a two-link underactuated highly nonlinear nonminimum-phase robot dynamics, [6]; Dang *et al.* conducted a real-time SDRE experiment for the swing-up and balance of a single inverted pendulum on a linear track, [7]; additionally, Menon *et al.* investigated the challenges associated with real-time implementation of SDRE control laws using *Schur* and *Kleinman* algorithms on five state variables system, [8].
The rest of the paper is organized as follows. In section 2 the SDRE controller for nonlinear optimal regulation is presented, reviewing some aspects on the SDC parameterization and an approximated technique for SDRE solution determination, referred to as Power Series Formulation (PSF). In section 3 the relative orbital dynamics is presented, wherein the relevant coordinate frames, governing equations of motion and standing assumptions are detailed. In section 4 the testing platform developed by DLR-Institute of Space Systems is detailed. Finally, the most relevant experimental results pointing out the effectiveness of SDRE approach are discussed.

2. State-Dependent Riccati Equation Technique

The SDRE strategy provides an effective and systematic algorithm to synthesize nonlinear feedback control by allowing nonlinearities in the system state. It is simply an extension of the constant-valued ARE used to find the optimal feedback control in the Linear Quadratic Regulator (LQR) problem.
Let consider the class of nonlinear in the state, affine in the input, continuous-time systems described by the following:

$$\begin{aligned} \dot{\boldsymbol{x}}(t) &= \boldsymbol{f}(\boldsymbol{x}(t)) + \boldsymbol{g}(\boldsymbol{x}(t))\boldsymbol{u}(t) \\ \boldsymbol{x}(0) &= \boldsymbol{x}_0 \end{aligned} \tag{1}$$

with the state vector $\boldsymbol{x} \in \boldsymbol{\Omega} \subseteq \Re^n$ and control $\boldsymbol{u} \in \Re^m$, such that $\boldsymbol{f} : \Re^n \to \Re^n$ and $\boldsymbol{g} : \Re^n \to \Re^{nxm}$. The SDRE method approaches the problem by mimicking the LQR formulation for linear systems. Accordingly, the system of Eq. (1) can be written in a like-linear form as follows:

$$\begin{aligned} \dot{\boldsymbol{x}}(\boldsymbol{t}) &= \boldsymbol{A}(\boldsymbol{x})\boldsymbol{x} + \boldsymbol{B}(\boldsymbol{x})\boldsymbol{U} \\ \boldsymbol{x}(0) &= \boldsymbol{x}_0 \end{aligned} \tag{2}$$

where $\boldsymbol{f}(\boldsymbol{x}) = \boldsymbol{A}(\boldsymbol{x})\boldsymbol{x}$ and $\boldsymbol{g}(\boldsymbol{x}) = \boldsymbol{B}(\boldsymbol{x})$, with $\boldsymbol{A}(\boldsymbol{x}) : \boldsymbol{\Omega} \to \Re^{nxn}$. The state-dependent dynamic matrix, $\boldsymbol{A}(\boldsymbol{x})$, is obtained by mathematical factorization and it is non-unique when $n>1$. It is worth noting that the former parameterization, known as *SDC*

parameterization or *extended linearization*, is possible if and only if the following conditions are satisfied, [9]:

- Condition 1. $\boldsymbol{f}(\boldsymbol{x}) = \boldsymbol{0}$ and $\boldsymbol{g}(\boldsymbol{x}) \neq \boldsymbol{0} \ \forall \ \boldsymbol{x}$
- Condition 2. $\boldsymbol{f}(\boldsymbol{x}) \in C^k$

The optimal control problem is to find a state feedback control $\boldsymbol{U}$ which minimizes the cost functional for all possible initial conditions $\boldsymbol{x}_0$,

$$J(\boldsymbol{x}_0, \boldsymbol{U}) = \frac{1}{2}\int_0^\infty (\boldsymbol{x}^T \boldsymbol{Q}(\boldsymbol{x})\boldsymbol{x} + \boldsymbol{U}^T \boldsymbol{Z}(\boldsymbol{x})\boldsymbol{U})dt \tag{3}$$

where the state and input weighting matrices are assumed state-dependent, such that $\boldsymbol{Q}(\boldsymbol{x}) : \Re^n \rightarrow \Re^{nxn}$ and $\boldsymbol{Z}(\boldsymbol{x}) : \Re^n \rightarrow \Re^{nxm}$, and positive semi-definite (PSD) and positive definite (PD) respectively for all $\boldsymbol{x}$ in order to ensure the local stability, [4].

If the pairs $\{\boldsymbol{A}(\boldsymbol{x}), \boldsymbol{B}(\boldsymbol{x})\}$ and $\{\boldsymbol{A}(\boldsymbol{x}), \boldsymbol{Q}(\boldsymbol{x})^{1/2}\}$ are respectively point-wise stabilizable and detectable extended linearization of the nonlinear system in the linear sense for all $\boldsymbol{x} \in \boldsymbol{\Omega}$, the approximated solution of minimizing of the infinite-time performance criterion, J, is given by the following expression:

$$\begin{aligned} \boldsymbol{U} &= -\boldsymbol{K}(\boldsymbol{x})\boldsymbol{x} \\ \boldsymbol{K}(\boldsymbol{x}) &= \boldsymbol{Z}^{-1}(\boldsymbol{x})\boldsymbol{B}^T(\boldsymbol{x})\boldsymbol{P}(\boldsymbol{x}) \end{aligned} \tag{4}$$

where $\boldsymbol{K}(\boldsymbol{x}) \in C^0(\boldsymbol{\Omega})$ and $\boldsymbol{P}(\boldsymbol{x}) \in \Re^{nxn}$ is the unique, symmetric, positive-definite solution of the continuous-time state-dependent Riccati equation,

$$\boldsymbol{P}(\boldsymbol{x})\boldsymbol{A}(\boldsymbol{x}) + \boldsymbol{A}^T(\boldsymbol{x})\boldsymbol{P}(\boldsymbol{x}) - \boldsymbol{P}(\boldsymbol{x})\boldsymbol{B}(\boldsymbol{x})\boldsymbol{Z}^{-1}(\boldsymbol{x})\boldsymbol{B}(\boldsymbol{x})^T\boldsymbol{P}(\boldsymbol{x})\boldsymbol{x} + \boldsymbol{Q}(\boldsymbol{x}) = 0 \tag{5}$$

Therefore, the SDRE solution for the infinite-time horizon nonlinear regulator problem (2)-(3) can be interpreted as a generalization of the infinite-time horizon time-invariant LQR problem, where all matrices are state-dependent. The main advantages of SDRE technique are simplicity and effectiveness, since no solution of the Hamilton-Jacobi-Bellman (HJB) partial differential equation is required to solve the infinite-horizon non-linear regulator problem, and design flexibility due to the possibility of tuning the state and input weighting matrices, $\boldsymbol{Q}$ and $\boldsymbol{Z}$, possibly depending on current state.

Equation (5) can be solved by different numerical algorithms, [10]; *Power Series Formulation (PSF)* allows to compute an approximation of the solution of Eq. (5) with a low computational effort and therefore it is exploited in our work, [5]. This approach consists in taking a power series expansion for $\boldsymbol{P}(\boldsymbol{x})$ in Eq.(5) in terms of a temporary variable $\boldsymbol{\varepsilon}$, such that, [3], [11]:

$$\boldsymbol{P}(\boldsymbol{x}) = \sum_{k=0}^{\infty} \boldsymbol{\varepsilon}^k \boldsymbol{P}_k \cong \sum_{k=0}^{I} \boldsymbol{\varepsilon}^k \boldsymbol{P}_k \tag{6}$$

and splitting the dynamic matrices $\boldsymbol{A}(\boldsymbol{x})$ and $\boldsymbol{B}(\boldsymbol{x})$ into constant and state-dependent part as,

$$\boldsymbol{A}(\boldsymbol{x}) = \boldsymbol{A}_0 + \varepsilon\boldsymbol{\Delta A}(\boldsymbol{x}); \qquad \boldsymbol{B}(\boldsymbol{x}) = \boldsymbol{B}_0 + \varepsilon\boldsymbol{\Delta B}(\boldsymbol{x}) \tag{7}$$

Substituting equations (6)-(7) in Eq. (5), the PSF procedure leads to the following expressions:

$$\boldsymbol{P}_0\boldsymbol{A}_0 + \boldsymbol{A}_0^T\boldsymbol{P}_0 - \boldsymbol{P}_0\boldsymbol{B}_0\boldsymbol{Z}^{-1}\boldsymbol{B}_0^T\boldsymbol{P}_0 + \boldsymbol{Q} = 0 \tag{8}$$

$$
\begin{aligned}
\tilde{\boldsymbol{A}}_0 &= (\boldsymbol{A}_0 - \boldsymbol{B}_0 \boldsymbol{Z}^{-1} \boldsymbol{B}_0^T \boldsymbol{P}_0) \\
\boldsymbol{P}_k \tilde{\boldsymbol{A}}_0 + \tilde{\boldsymbol{A}}_0^T \boldsymbol{P}_k &= -\boldsymbol{P}_{k-1} \boldsymbol{\Delta A}(\boldsymbol{x}) - \boldsymbol{\Delta A}(\boldsymbol{x})^T \boldsymbol{P}_{k-1} + \qquad k = 1,\ldots,l \\
&\quad + \sum_{j=0}^{k-1} \boldsymbol{P}_j (\boldsymbol{B}_0 \boldsymbol{Z}^{-1} \boldsymbol{\Delta B}(\boldsymbol{x})^T + \boldsymbol{\Delta B}(\boldsymbol{x}) \boldsymbol{Z}^{-1} \boldsymbol{B}_0) \boldsymbol{P}_{k-1-j} + \\
&\quad + \sum_{j=1}^{k-1} \boldsymbol{P}_j (\boldsymbol{B}_0 \boldsymbol{Z}^{-1} \boldsymbol{B}_0^T) \boldsymbol{P}_{k-j} + \sum_{j=0}^{k-2} \boldsymbol{P}_j (\boldsymbol{\Delta B}(\boldsymbol{x}) \boldsymbol{Z}^{-1} \boldsymbol{\Delta B}(\boldsymbol{x})^T) \boldsymbol{P}_{k-2-j}
\end{aligned} \tag{9}
$$

Note that the PSF method reduces the SDRE control problem to the solution of an off-line algebraic Riccati equation (see Eq. (8)) plus a series of linear Lyapounv equations (see Eqs. (9)) that might be solved through linear algebra manipulation, as discussed in [12], [13] and [5], or more efficiently by Bartles and Stweart algorithm, presented in [14] and [10]. Even though the PSF method is effective also when the state and input weighting matrices, $\boldsymbol{Q}$ and $\boldsymbol{Z}$, depend on the state vector $\boldsymbol{x}$, it would require more computational efforts to find the stabilizing solution, since Eq. (8) should be determined at each instant time; therefore, without loss of generality, in our study the matrices $\boldsymbol{Q}$ and $\boldsymbol{Z}$ are considered constant.

3. Relative Dynamics

3.1. Cartesian Coordinate Frames

In order to describe the relative coupled motion between two satellites, the following reference frames are defined (see Figure 1).

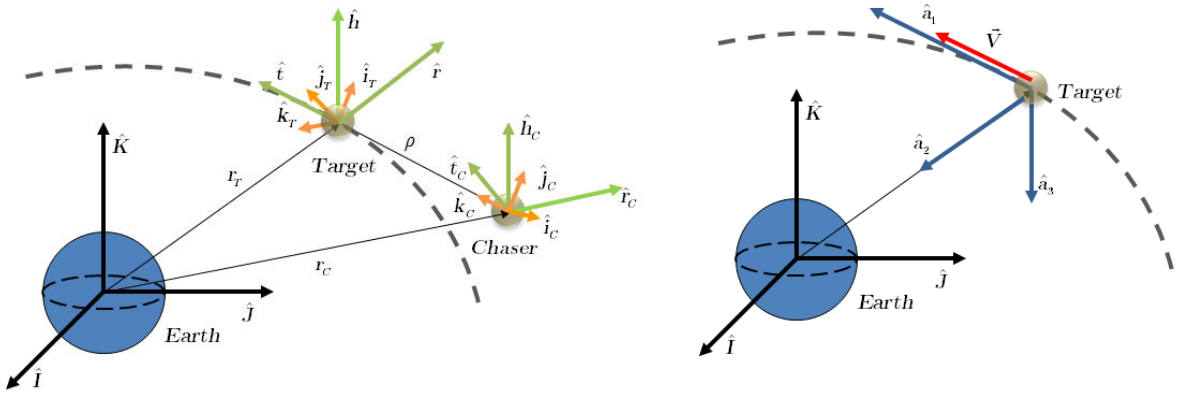

(a) (b)

Figure 1. Reference frames: a) ORFs and BRRs; b) LVLHF.

Earth centered inertial (ECI). ECI, denoted as $\boldsymbol{N}$, is centered in Earth and it has $\hat{\boldsymbol{K}}$ versor aligned with Earth rotation axis (towards the north pole), $\hat{\boldsymbol{I}}$ directed towards the vernal equinox and $\hat{\boldsymbol{J}}$ completes the right-handed orthogonal reference frame.
Orbital reference frame (ORF). ORFs, named $\boldsymbol{O}_C$ and $\boldsymbol{O}_T$ for chaser and target satellites respectively, are centered in the centre of mass of each satellite and they have the versors $\hat{\boldsymbol{r}}$ and $\hat{\boldsymbol{h}}$ aligned with radial direction and orbital angular momentum respectively; $\hat{\boldsymbol{t}}$ versor completes the right-handed orthogonal reference frame.

Whenever the ORF is attached to the target satellite centre of mass, it is denoted as ***H*** and known as *Hill reference frame*.
Local vertical/local horizontal frame (LVLHF). LVLHF is centered in the centre of mass of the target spacecraft and it has $\hat{\boldsymbol{a}}_3$ versor directed along the opposite direction of the angular momentum vector of the target orbit, $\hat{\boldsymbol{a}}_2$ versor aligned with the zenith direction (outward direction from the target satellite) and $\hat{\boldsymbol{a}}_1 = \hat{\boldsymbol{a}}_2 \times \hat{\boldsymbol{a}}_3$ ($\hat{\boldsymbol{a}}_1$ is in the direction of the orbital velocity vector but not necessary aligned with it). In R&D literature the versors $\hat{\boldsymbol{a}}_1$, $\hat{\boldsymbol{a}}_2$ and $\hat{\boldsymbol{a}}_3$ are named respectively *V-bar*, *R-bar* and *H-bar*, (see Figure 1 (b)).
Body Reference frame (BRF). These frames, denoted as ***C*** and ***T*** for chaser and target satellites respectively, are located in the centre of mass of each spacecraft and the axes are oriented as the inertia principal axes. Without loss of generality, we assume that $\hat{\boldsymbol{j}}_C$ and $-\hat{\boldsymbol{j}}_T$ are designed to be the outward direction of the chaser and target docking port.

3.2. Translational Relative Dynamics

The relative translational dynamic equations are based on the definition of relative position and velocity with respect to Hill reference frame. Therefore, let us define the relative position and velocity vectors as follows (see Figure 1 (a)):

$$\begin{aligned} \boldsymbol{\rho} &= x\hat{\boldsymbol{r}} + y\hat{\boldsymbol{t}} + z\hat{\boldsymbol{h}} \\ \dot{\boldsymbol{\rho}} &= \dot{x}\hat{\boldsymbol{r}} + \dot{y}\hat{\boldsymbol{t}} + \dot{z}\hat{\boldsymbol{h}} \end{aligned} \tag{10}$$

Then, the relative translational dynamics is governed by the following equations

$$\begin{aligned} \ddot{\boldsymbol{\rho}} &= -2\left[\boldsymbol{\omega}_{H,I}^{H} \wedge\right]\dot{\boldsymbol{\rho}} - \left[\boldsymbol{\omega}_{H,I}^{H} \wedge\right]\left[\boldsymbol{\omega}_{H,I}^{H} \wedge\right]\boldsymbol{\rho} - \left[\dot{\boldsymbol{\omega}}_{H,I}^{H} \wedge\right]\boldsymbol{\rho} + \Delta\boldsymbol{f}_{grav}^{H} + \boldsymbol{f}_{control}^{H} \\ \Delta\boldsymbol{f}_{grav}^{H} &= \boldsymbol{f}_{grav,C}^{H} - \boldsymbol{f}_{grav,T}^{H} = -\frac{\mu}{\left\|\boldsymbol{r}_T + \boldsymbol{\rho}^{H}\right\|^3}\left(\boldsymbol{r}_T^{H} + \boldsymbol{\rho}^{H}\right) + \frac{\mu}{\left\|\boldsymbol{r}_T\right\|^3}\left(\boldsymbol{r}_T^{H}\right) \end{aligned} \tag{11}$$

where $[\cdot \wedge]$ denotes the cross product matrix and $\boldsymbol{f}_{control}^{H} \in \Re^3$ is the control acceleration. If the target spacecraft moves on a circular orbit around the Earth, the evolution of r_T and $\boldsymbol{\omega}_{H,I}^{H}$ is given by

$$\dot{\boldsymbol{\omega}}_{H,I}^{H} = 0 \qquad \boldsymbol{\omega}_{H,I}^{H} = \frac{h}{r_T^2}\hat{\boldsymbol{h}} \quad \dot{r}_T = 0 \tag{12}$$

where h is the modulus of the orbital angular momentum, and Eq. (11) can be further simplified.

3.3. Rotational Relative Dynamics

Using the quaternion parameterization, $\boldsymbol{q}_e = [q_{0e}, q_{1e}, q_{2e}, q_{3e}]^{\mathrm{T}}$, to represent the relative attitude between the chaser and target BRFs, the kinematical equation of motion is given by:

$$\dot{\boldsymbol{q}}_e = \begin{Bmatrix} \dot{q}_{0,e} \\ \dot{\bar{\boldsymbol{q}}}_e \end{Bmatrix} = \frac{1}{2}\begin{bmatrix} 0 & -\{\boldsymbol{\omega}_{C,T}^C\}^T \\ \{\boldsymbol{\omega}_{C,T}^C\} & \left[\boldsymbol{\omega}_{C,T}^C \wedge\right] \end{bmatrix}\boldsymbol{q}_e \tag{13}$$

The vector $\boldsymbol{\omega}_{C,T}^C$ represents the relative angular velocity of ***C*** with respect to ***T***, and it can be expressed as

$$\boldsymbol{\omega}_{C,T}^C = \boldsymbol{\omega}_{C,I}^C - \boldsymbol{S}_T^C(\boldsymbol{q}_e)\boldsymbol{\omega}_{T,I}^T \tag{14}$$

where $\boldsymbol{S}_T^C(\boldsymbol{q}_e)$ is the transformation matrix which describes the orientation of the chaser BRF relative to the target BRF, [15]. Thus, the time derivative of Eq. (14) leads to

$$\dot{\boldsymbol{\omega}}_{C,T}^C = \dot{\boldsymbol{\omega}}_{C,I}^C - \boldsymbol{S}_T^C(\boldsymbol{q}_e)\dot{\boldsymbol{\omega}}_{T,I}^T - \dot{\boldsymbol{S}}_T^C(\boldsymbol{q}_e)\boldsymbol{\omega}_{T,I}^T = \dot{\boldsymbol{\omega}}_{C,I}^C - \boldsymbol{S}_T^C(\boldsymbol{q}_e)\dot{\boldsymbol{\omega}}_{T,I}^T + \left[\boldsymbol{\omega}_{C,T}^C \wedge\right]\boldsymbol{S}_T^C(\boldsymbol{q}_e)\boldsymbol{\omega}_{T,I}^T \tag{15}$$

In our study we assume that the target satellite is controlled such that its BRF coincides with Hill reference frame and its center of mass moves on a Earth circular orbit; thus the Eq. (15) can be rearranged as

$$\begin{aligned} \dot{\boldsymbol{\omega}}_{C,H}^C = \boldsymbol{I}_C^{-1}\Big(-\Big[\Big(\boldsymbol{\omega}_{C,H}^C + \boldsymbol{S}_H^C(\boldsymbol{q}_e)\boldsymbol{\omega}_{H,I}^H\Big)\wedge\Big]\boldsymbol{I}_C\Big(\boldsymbol{\omega}_{C,T}^C + \boldsymbol{S}_H^C(\boldsymbol{q}_e)\boldsymbol{\omega}_{H,I}^H\Big) + \boldsymbol{T}_{ext}^C\Big) + \\ -\Big[\boldsymbol{S}_H^C(\boldsymbol{q}_e)\boldsymbol{\omega}_{H,I}^H \wedge\Big]\boldsymbol{\omega}_{C,H}^C \end{aligned} \tag{16}$$

being

$$\begin{aligned} &\boldsymbol{\omega}_{C,H}^C = \boldsymbol{\omega}_{C,T}^C && \boldsymbol{\omega}_{H,I}^H = \boldsymbol{\omega}_{T,I}^T \quad \boldsymbol{S}_H^C(\boldsymbol{q}_e) = \boldsymbol{S}_T^C(\boldsymbol{q}_e) \\ &\dot{\boldsymbol{\omega}}_{C,I}^C = \boldsymbol{I}_C^{-1}\left(-\boldsymbol{\omega}_{C,I}^C \wedge \boldsymbol{I}_C\boldsymbol{\omega}_{C,I}^C + \boldsymbol{T}_{ext}^C\right) && \dot{\boldsymbol{\omega}}_{H,I}^H = 0 \end{aligned} \tag{17}$$

where $\boldsymbol{I}_C$ represents the inertia dyadic about the chaser body's center of gravity. Note that only the disturbing torques due to the gravitational field are considered in Eq.(17), such that

$$\begin{aligned} \boldsymbol{T}_{ext}^C &= 3\frac{\mu}{\left\|\boldsymbol{r}_C^C\right\|^5}\left[\boldsymbol{r}_C^C \wedge\right]\boldsymbol{I}_C\boldsymbol{r}_C^C + \boldsymbol{T}_{control}^C \\ \boldsymbol{r}_C^C &= \boldsymbol{S}_H^C(\boldsymbol{q}_e)\left(\boldsymbol{r}_T^H + \boldsymbol{\rho}^H\right) \end{aligned} \tag{18}$$

where $\boldsymbol{T}_{control}^C \in \Re^3$ is the control torque. In addition, according with above hypothesis, the kinematic equation (13) can be written as,

$$\begin{aligned} \dot{\boldsymbol{q}}_e = \begin{Bmatrix} \dot{q}_{0,e} \\ \dot{\bar{\boldsymbol{q}}}_e \end{Bmatrix} = \frac{1}{2}\begin{bmatrix} 0 & -\{\boldsymbol{\omega}_{C,H}^C\}^T \\ \{\boldsymbol{\omega}_{C,H}^C\} & \left[\boldsymbol{\omega}_{C,H}^C \wedge\right] \end{bmatrix}\boldsymbol{q}_e = \frac{1}{2}\begin{bmatrix} -\bar{\boldsymbol{q}}_e \\ q_{0,e}\boldsymbol{I}_{3x3} + \left[\bar{\boldsymbol{q}}_e \wedge\right] \end{bmatrix}\boldsymbol{\omega}_{C,H}^C = \\ \begin{bmatrix} -\bar{\boldsymbol{q}}_e \\ q_{0,e}\boldsymbol{I}_{3x3} + \left[\bar{\boldsymbol{q}}_e \wedge\right] \end{bmatrix}\boldsymbol{\omega}_{C,I}^C - \frac{1}{2}\begin{bmatrix} 0 & -\{\boldsymbol{S}_H^C(\boldsymbol{q}_e)\boldsymbol{\omega}_{H,I}^H\}^T \\ \{\boldsymbol{S}_H^C(\boldsymbol{q}_e)\boldsymbol{\omega}_{H,I}^H\} & -\left[\boldsymbol{S}_H^C(\boldsymbol{q}_e)\boldsymbol{\omega}_{H,I}^H \wedge\right] \end{bmatrix}\boldsymbol{q}_e \end{aligned} \tag{19}$$

4. Rendezvous and Docking Testbed

The R&D testbed designed by *DLR - Institute of Space Systems*, referred to as TEAMS (Test Environment for Application of Multiple Spacecraft), consists of a frictionless granite table (about 4x5 m) with several air cushion vehicles moving on it. Each vehicle floats thanks to a set of air bearing pads, reproducing a frictionless and weightless

environment in two dimension and three degree of freedom, and it is equipped by six proportional thrusters for its motion which are controlled by a pulse-width modulation (PWM) signal generated by a dedicated microcontroller. Each vehicle consists of two parts (see Figure 2). The lower part, referred to as Transport Platform (TP), is devoted to contain the 300 bar air tanks and the pressure regulators to support the pads and proportional thrusters with pressurized air. On the top of the TP the second stage, referred to as Attitude Platform (AP), is constrained such that no relative motion between two parts is permitted. On the AP sensors, actuators and electronic equipments are located such that the position of the center of mass of the vehicle is not far from the junction point of the two stages. The vehicles are completely autonomous: the air supply system supports the air cushion pads and the proportional thrusters with pressurized air; an on-board computer allows to process data coming from sensors as well as to drive the actuators; moreover a battery package and a power distribution unit (PDU) supply all electronics components. The onboard computer is a PC104 stacked with several boards with a x86 Atom Z530 processor (1.6 GHz). A real-time operating system (RTOS) QNX is used for the onboard computer; this comes with integrated development environment (IDE) based on the open-source IDE Eclipse and with C/C++ compiler based on GNU C-compiler, making the integration with Matlab/Simulink/RTW easy.
In order to determine the position and attitude of the vehicle a DTrack infrared tracking system is exploited. It consists mainly of 3 components: i) the tracking PC; ii) 6 cameras and iii) up to 20 targets. The cameras emit infrared flashes with a frequency of 60 Hz which are reflected by the target (a set of reflective balls, named markers) installed on board of the vehicle; the reflected signal is captured by the cameras and handled by tracking PC which compute the navigation solution and, subsequently, broadcast it on the local network. For more details on the status of the facility and on its future developments, we address the reader to [16].

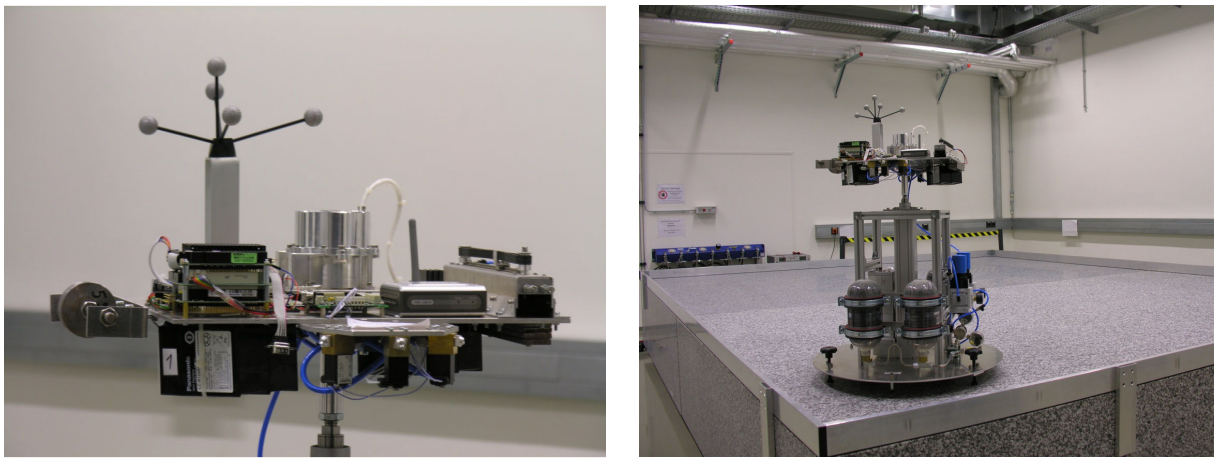

a) b)

Figure 2. TEAMS facility overview: a) AP layout; b) assembled vehicle.

4.1. Testbed Functional Architecture

In Figure 3 the functional scheme of TEAMS platform is depicted. The DTrack system is exploited to compute the position and the orientation of the moving vehicle with respect to a fixed reference frame placed in the middle of the granite table. This information, obtained by using a dedicated computer as discussed in previous subsection, is transferred to the vehicle via the wifi network. The guidance, navigation and control solution is calculated by the on-board computer and sent to the thrusters control board for commanding the six actuators.
It is worth noting that only one vehicle is used during the experimental campaign to emulate the R&D manoeuvre. From a dynamical standpoint, this fact doesn't affect the R&D manoeuvring simulation; in fact, in our simulated scenario, the relative motion between the target BRF and Hill reference frame is ignored.

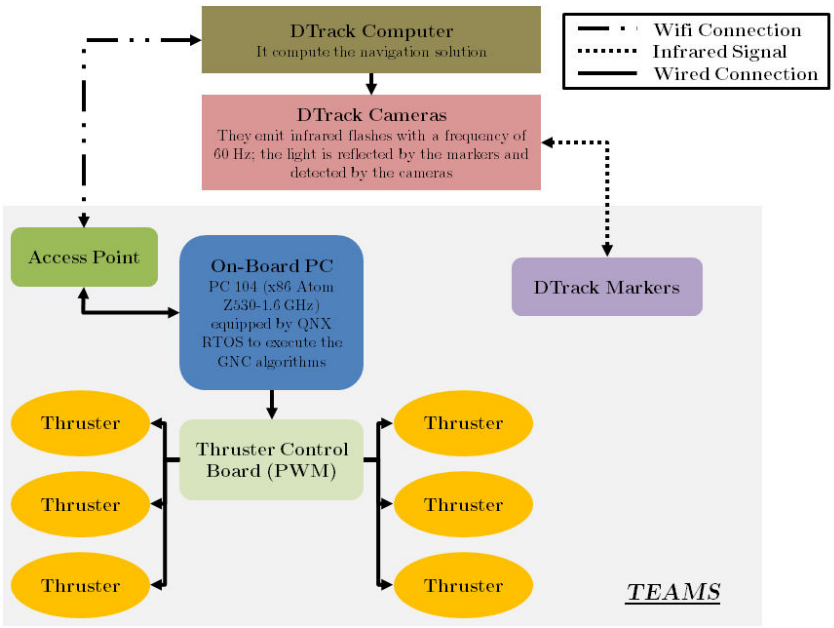

Figure 3. TEAMS functional architecture.

4.2. Orbital Motion Simulation on the Testbed

In order to emulate the orbital dynamics of the chaser satellite relative to the Hill reference frame by using the presented testbed, it is necessary that the vehicle actuator system generates the inertia acceleration/torque due to the orbital motion of Hill reference frame and the gravitational force/torque, besides the control signal. Moreover, both the provided inertia and control acceleration/torque have to be scaled to satisfy the facility constrains.
For sake of clarity, let us derive the equations of motion of the vehicle moving on the frictionless surface as (see Figure 4),

$$\begin{aligned} \ddot{\boldsymbol{r}}_V^{HT} &= \boldsymbol{f}_{Thrust}^{HT} \\ \dot{\boldsymbol{\omega}}_{V,HT}^{V} &= \boldsymbol{I}_V^{-1}\left(-\left[\boldsymbol{\omega}_{V,HT}^{V}\wedge\right]\boldsymbol{I}_V\boldsymbol{\omega}_{V,HT}^{HT} + \boldsymbol{T}_{Thrust}^{V}\right) \end{aligned} \tag{20}$$

where $\boldsymbol{f}_{Thrust}^{HT} \in \Re^3$ and $\boldsymbol{T}_{Thrust}^{V} \in \Re^3$ are respectively the accelerations and the torques provided by the thrusters expressed in inertial reference frame, ***HT***, and vehicle fixed reference frame, ***V***; $\boldsymbol{\omega}_{V,HT}^{V}$ is the angular rate of the vehicle fixed reference frame and $\boldsymbol{I}_V$ is the inertia matrix of the vehicle.

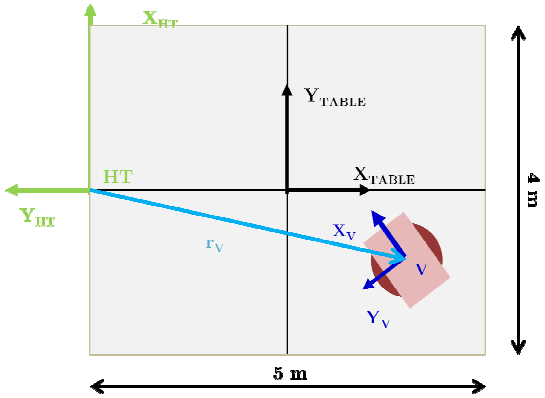

Figure 4. Layout of testbed.

In order that Eq. (20) correspond to the Eqs. (11)-(16) the terms $\boldsymbol{f}_{Thrust}^{HT}$ and $\boldsymbol{T}_{Thrust}^{V}$ must to be set to

$$\begin{aligned}
\boldsymbol{f}_{Thrust}^{HT} &= -\left[\dot{\breve{\boldsymbol{\omega}}}_{H,I}^{H} \wedge\right]\breve{\boldsymbol{\rho}}^{H} - 2\left[\breve{\boldsymbol{\omega}}_{H,I}^{H} \wedge\right]\dot{\breve{\boldsymbol{\rho}}}^{H} - \left[\breve{\boldsymbol{\omega}}_{H,I}^{H} \wedge\right]\left[\breve{\boldsymbol{\omega}}_{H,I}^{H} \wedge\right]\breve{\boldsymbol{\rho}}^{H} + \Delta\breve{\boldsymbol{f}}_{grav}^{H} + \breve{\boldsymbol{f}}_{control,C}^{H} \\
\boldsymbol{T}_{Thrust}^{V} &= \boldsymbol{I}_V\left(\breve{\boldsymbol{I}}_C^{-1}\left(-\left[\breve{\boldsymbol{\omega}}_{C,I}^{C} \wedge\right]\breve{\boldsymbol{I}}_C\breve{\boldsymbol{\omega}}_{C,I}^{C} + \breve{\boldsymbol{T}}_{grav}^{C} + \breve{\boldsymbol{T}}_{control}^{C}\right) - \boldsymbol{S}_H^C\dot{\breve{\boldsymbol{\omega}}}_{H,I}^{H} - \left[\boldsymbol{S}_H^C\breve{\boldsymbol{\omega}}_{H,I}^{H} \wedge\right]\breve{\boldsymbol{\omega}}_{C,H}^{C}\right) \\
&\quad + \left[\boldsymbol{\omega}_{V,HT}^{V} \wedge\right]\boldsymbol{I}_V\boldsymbol{\omega}_{V,H}^{V} \qquad (21) \\
\Delta\breve{\boldsymbol{f}}_{grav}^{H} &= \breve{\boldsymbol{f}}_{grav,C}^{H} - \breve{\boldsymbol{f}}_{grav,T}^{H} = -\frac{\breve{\mu}}{\left\|\breve{\boldsymbol{r}}_T^{H} + \breve{\boldsymbol{\rho}}^{H}\right\|^3}\left(\breve{\boldsymbol{r}}_T^{H} + \breve{\boldsymbol{\rho}}^{H}\right) + \frac{\breve{\mu}}{\left\|\breve{\boldsymbol{r}}_T^{H}\right\|^3}\left(\breve{\boldsymbol{r}}_T^{H}\right) \\
\breve{\boldsymbol{T}}_{grav}^{C} &= -\frac{\breve{\mu}}{\left\|\breve{\boldsymbol{r}}_T^{H} + \breve{\boldsymbol{\rho}}^{H}\right\|^5}\left[\left(\boldsymbol{S}_H^C(\boldsymbol{q}_e)\left(\breve{\boldsymbol{r}}_T^{H} + \breve{\boldsymbol{\rho}}^{H}\right)\right) \wedge\right]\breve{\boldsymbol{I}}_C\left(\boldsymbol{S}_H^C(\boldsymbol{q}_e)\left(\breve{\boldsymbol{r}}_T^{H} + \breve{\boldsymbol{\rho}}^{H}\right)\right)
\end{aligned}$$

where the superscript "˘" indicates the scaled variable. From (21), it is evident that equations Eq. (20) coincides with Eqs. (11)-(16) if

$$\breve{\boldsymbol{\rho}}^{H} = \boldsymbol{r}_V^{HT} \quad \dot{\breve{\boldsymbol{\rho}}}^{H} = \boldsymbol{r}_V^{HT} \quad \breve{\boldsymbol{\omega}}_{C,H}^{C} = \boldsymbol{\omega}_{V,HT}^{V} \quad \breve{\boldsymbol{q}}_e = \boldsymbol{q}_{V,HT} \qquad (22)$$

and

$$\begin{aligned}
\breve{\boldsymbol{\rho}}^{H} &= \boldsymbol{\rho}^{H} m \qquad \dot{\breve{\boldsymbol{\rho}}}^{H} = \dot{\boldsymbol{\rho}}^{H} m / t \qquad \breve{\boldsymbol{r}}_T^{H} = \boldsymbol{r}_T^{H} m \\
\breve{\boldsymbol{\omega}}_{C,H}^{C} &= \boldsymbol{\omega}_{C,H}^{C} / t \qquad \dot{\breve{\boldsymbol{\omega}}}_{C,H}^{C} = \dot{\boldsymbol{\omega}}_{C,H}^{C} / t^2 \qquad \breve{\boldsymbol{\omega}}_{H,I}^{H} = \boldsymbol{\omega}_{H,I}^{H} / t \qquad (23) \\
\breve{\boldsymbol{I}}_C &= \boldsymbol{I}_C k m^2 \qquad \breve{\mu} = \mu m^3 / t^2
\end{aligned}$$

where *m*, *t*, and *k* are length, time and mass scale factors defined such that:

- the scaled chaser satellite mass is equal to the floating vehicle mass;
- the maximum scaled relative position doesn't overcome the testbed dimension;

– the vehicle completes the maneuver within the maximum autonomy time, due to the time needed to empty the air pressurized tanks of floating system and to discharge the onboard batteries.

5. Hardware Experiment

This section presents results from hardware experiments in order to prove the effectiveness of the proposed SDRE nonlinear controller; particularly, experimental campaign provides confidence that all critical issues are addressed, and that the proposed nonlinear methodology can be implemented on a real hardware.

5.1. Simulated Scenario

The TEAMS platform described in section 4 is used for emulation of a close range R&D manoeuvre between two satellites orbiting the Earth. More specifically, in our study the target spacecraft is assumed to be controlled such that its orbital motion is Keplerian and its BRF is oriented as the Hill reference frame; furthermore the chaser satellite has to approach the target tracking a planar trajectory consisting of one hop and a forced motion along the V-bar direction, besides to allow the alignment of docking mechanisms. The reference relative position and velocity vector for hopping phase are provided by the analytical solution of Hill-Clohessy-Wiltshire equations, [17], [18]; differently, a specific velocity profile is implemented for the final forced approaching phase in order to achieve the desired relative position and velocity in a fixed interval time, [19]. In Figure 5 the scaled reference trajectories sketched on the frictionless surface is drawn. The Hill reference frame is represented by a fixed reference frame, referred to as ***HT***, on the testbed arena (see red axis X_{HT} and Y_{HT} in Figure 5): thus the vehicle moving on granite table has to follow the reference trajectory and align its Y_V-axis (see Figure 4) along the Y_{HT}-axis direction.

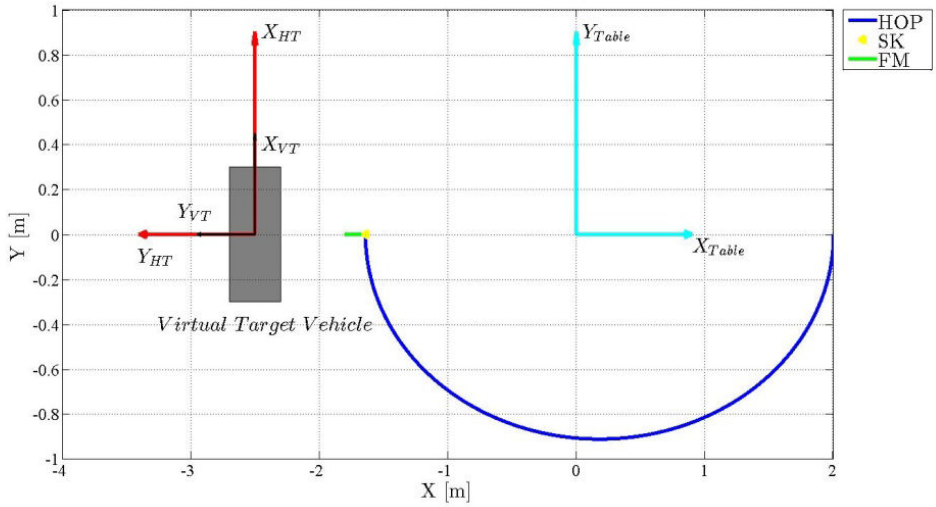

Figure 5. Reference trajectory on frictionless surface.

5.2. Controller Design

The synthesis of nonlinear controller is based on the dynamics and kinematics equations of relative orbital motion described in section 3. According with the SDRE formulation presented in section 2, the nonlinear control law is given by

$$\boldsymbol{U}(\boldsymbol{x}_{control}) = -\boldsymbol{Z}^{-1}\boldsymbol{B}^{T}\boldsymbol{P}(\boldsymbol{x}_{control})\left(\boldsymbol{x}_{control} - \boldsymbol{x}_{control,ref}\right) = -\boldsymbol{Z}^{-1}\boldsymbol{B}^{T}\boldsymbol{P}(\boldsymbol{x}_{control})\boldsymbol{e}$$

$$\boldsymbol{x}_{control,ref} = \left[\breve{\boldsymbol{\rho}}^{H}_{ref} \quad \dot{\breve{\boldsymbol{\rho}}}^{H}_{ref} \quad s \quad \breve{\boldsymbol{\omega}}^{C}_{C/I,ref} \quad \breve{\boldsymbol{q}}_{e,ref}\right]^{T} \tag{24}$$

$$\boldsymbol{x}_{control} = \left[\breve{\boldsymbol{\rho}}^{H} \quad \dot{\breve{\boldsymbol{\rho}}}^{H} \quad s \quad \breve{\boldsymbol{\omega}}^{C}_{C/I} \quad \breve{\boldsymbol{q}}_{e}\right]^{T}$$

where s is a stable additional state needed to satisfy the condition 1 discussed in section 2, [1], [20]. The solution of algebraic Riccati equation, $\boldsymbol{P}(\boldsymbol{x}_{control})$, at each sample time is obtained by using the PSF algorithm presented in section 2. Finally, the controller object is to ensure that $\boldsymbol{e} \to 0$ whenever $t \to \infty$ (asymptotical stability).
Without loss of generality the input and state weighting matrices, $\boldsymbol{Z}(\boldsymbol{x})$ and $\boldsymbol{Q}(\boldsymbol{x})$, reported in cost functional (3) are chosen constant and set to

$$\boldsymbol{Q} = \begin{bmatrix} \boldsymbol{Q}_{11} & 0_{3\boldsymbol{x}3} & 0_{3\boldsymbol{x}1} & 0_{3\boldsymbol{x}3} & 0_{3\boldsymbol{x}4} \\ 0_{3\boldsymbol{x}3} & \boldsymbol{Q}_{22} & 0_{3\boldsymbol{x}1} & 0_{3\boldsymbol{x}3} & 0_{3\boldsymbol{x}4} \\ 0_{1\boldsymbol{x}3} & 0_{1\boldsymbol{x}3} & 0 & 0_{1\boldsymbol{x}3} & 0_{1\boldsymbol{x}4} \\ 0_{3\boldsymbol{x}3} & 0_{3\boldsymbol{x}3} & 0_{3\boldsymbol{x}1} & \boldsymbol{Q}_{33} & 0_{3\boldsymbol{x}4} \\ 0_{4\boldsymbol{x}3} & 0_{4\boldsymbol{x}3} & 0_{4\boldsymbol{x}1} & 0_{4\boldsymbol{x}3} & \boldsymbol{Q}_{44} \end{bmatrix} \quad \boldsymbol{Z} = \begin{bmatrix} \boldsymbol{Z}_{11} & 0_{3\boldsymbol{x}3} \\ 0_{3\boldsymbol{x}3} & \boldsymbol{Z}_{22} \end{bmatrix}$$

$$\begin{aligned} \boldsymbol{Q}_{11} &= diag([1\boldsymbol{e}\text{-}4 \quad 1\boldsymbol{e}\text{-}4 \quad 1\boldsymbol{e}\text{-}6]) && (1/m)^2 \\ \boldsymbol{Q}_{22} &= diag([10\boldsymbol{e}\text{-}2 \quad 10\boldsymbol{e}\text{-}2 \quad 10\boldsymbol{e}\text{-}4]) && (s/m)^2 \\ \boldsymbol{Q}_{33} &= \boldsymbol{I}_{3\boldsymbol{x}3}1\boldsymbol{e}-7 && (s)^2 \\ \boldsymbol{Q}_{44} &= \boldsymbol{I}_{4\boldsymbol{x}4}1\boldsymbol{e}-7 && (dim) \\ \boldsymbol{Z}_{11} &= \boldsymbol{I}_{3\boldsymbol{x}3}1.5 && (s^2/m)^2 \\ \boldsymbol{Z}_{22} &= diag([1\boldsymbol{e}\text{-}4 \quad 1\boldsymbol{e}\text{-}4 \quad 1\boldsymbol{e}\text{-}8]) && (s^2/kgm^2)^2 \end{aligned} \tag{25}$$

Note that the above matrices are referred to the orbital controller; this means that, they have to be scaled according with m, t, and k scaling factors.
Since the DTrack system provides only the relative position[1] and attitude of the vehicle, the relative velocity, $\dot{\breve{\boldsymbol{\rho}}}^{H}_{ref}$, and the angular rate, $\breve{\boldsymbol{\omega}}^{C}_{C/I}$, are determined by an Extended Kalman Filter based on the linearized form of Eqs. (11)-(16)-(19), [16].

5.3. Results

As previously discussed, the TEAMS testbed is exploited to simulate a close range R&D manoeuvre; particularly, the initial and final orbital relative position are

[1] The DTrack system provide the position and the attitude of the vehicle with respect to ***Table*** reference frame placed in the center of the table (see Figure 4). Anyhow, the position and the attitude of the vehicle relative to HT reference frame can be easily computed by a roto-traslation transformation.

$\boldsymbol{\rho}^{H}_{\mathrm{Re}f}(0) = [0 \quad -100 \quad 0]^T$ and $\boldsymbol{\rho}^{H}_{\mathrm{Re}f}(t_f) = [0 \quad -5 \quad 0]^T$ respectively, expressed in Hill reference frame.
In Table 1 the parameters required to scale the control, the inertial and the gravitational forces/torques are reported. Note that these values are related to the vehicle mass, to dimension of arena where vehicle moves and to the autonomy of the air pressured system, as discussed in subsection 4.2.

Testbed	Mass Scaling Factor	Length Scaling Factor	Time Scaling Factor
TEAMS	0.046	0.04	0.1877

Table 1. Scaling factors for close range R&D maneuver.

Note that the actuator system installed on TEAMS platform produces only the inertial and gravitational forces/torques, that is $\boldsymbol{f}^{HT}_{Thrust}$ and $\boldsymbol{T}^{V}_{Thrust}$, ignoring the perturbing forces/torques caused by the Earth oblateness and atmospheric drag. This choice is due to the order of magnitude of this orbital perturbing effects; in fact the scaled orbital perturbing forces/torques are smaller than the forces/torques due to the laboratory environment, i.e. the forces due to non leveled frictionless surface or the torques due to offset between center of gravity and point of conjunction between the two stages of the vehicle.
The following experimental results are referred to a fourth expansion order, *l*, for the PSF; in addition the SDRE controller runs at 10 Hz.
The entire orbital manoeuvre is simulated in 12 minutes; this is the time required by the air pressured tanks to be almost emptied.
In Figure 6-Figure 7 the relative position error, the relative velocity error, the absolute angular rate error and the relative quaternion error regarding the TEAMS vehicle motion are illustrated. It is worth noting that the SDRE controller guarantees the TEAMS floating vehicle to approach the virtual target vehicle following the defined trajectory; at the end of the maneuver the norm of relative position error is about 8.3e-3 *m* whereas the norm of relative velocity error is about 1.2e-3 *m/s*.

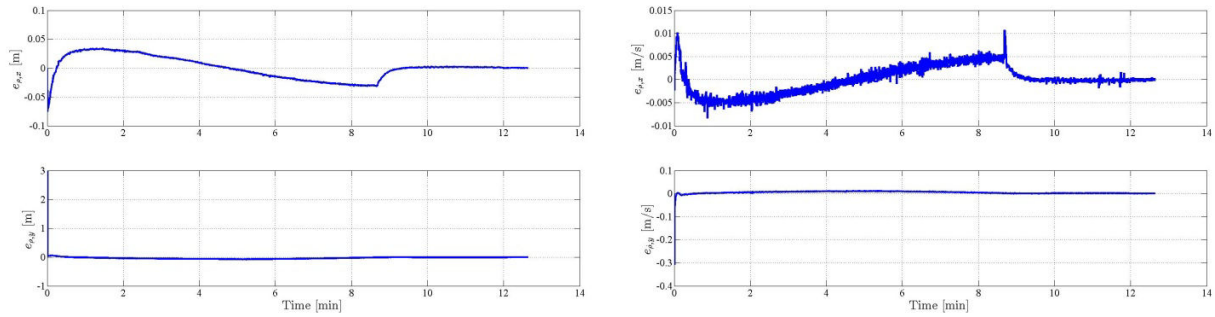

(a) (b)

Figure 6. Relative translational state error: a) relative position error; b) relative velocity error.

Note that the oscillation shown in absolute angular velocity error and relative quaternion error plots (at 4.6 minute) is due to a gap on the granite table which blocks up the transition of one air-pad, generating a disturbing torque. This phenomenon occurs

randomly and it was not significant in many experiments. Anyhow, also in presence of this environmental disturbing effect, the SDRE controller is able to nullify the relative attitude of the floating vehicle with respect to the virtual target vehicle, synchronizing the vehicles body-fixed reference frames.

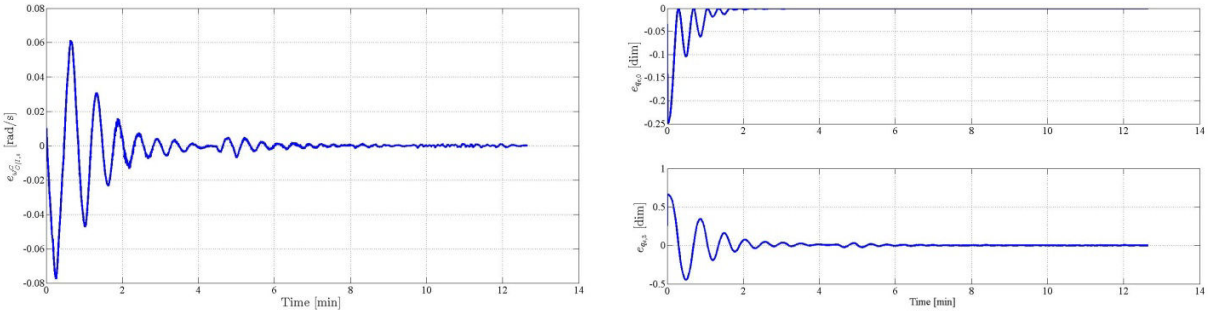

(a) (b)

Figure 7. Rotational error state vector: a) absolute angular velocity error; b) relative quaternion error.

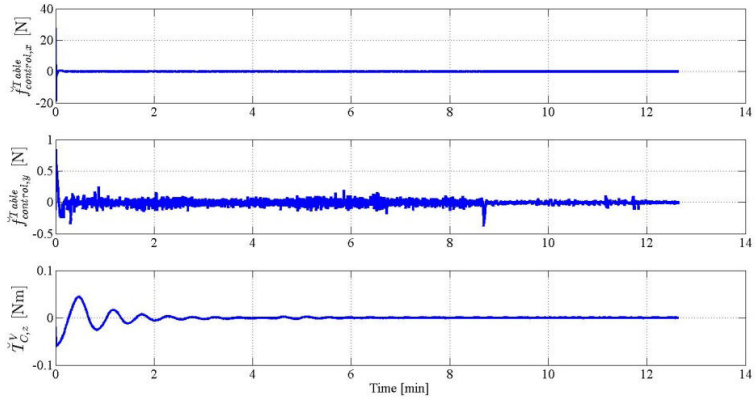

Figure 8. SDRE controller force/torque.

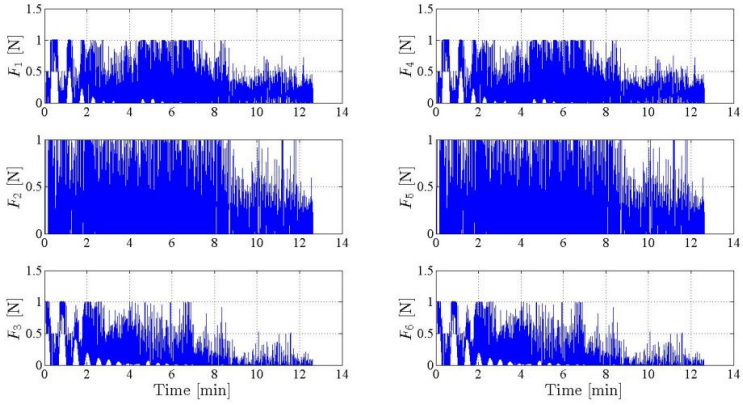

Figure 9. Thrust generated by each proportional thruster.

In Figure 8 the TEAMS control forces expressed in an inertial reference frame centered in the table, referred to as ***Table*** reference frame, and torque expressed in vehicle body-fixed reference frame are shown. Moreover, in Figure 9 the total thrust (normalized by the maximum thrust value) provided by each proportional actuator is illustrated.

Algorithm	Execution Time (s)
PSF (order l= 4)	0.063

Table 2. Execution time for SDRE algorithm.

Finally, In Table 2 the execution time required to compute the guidance, navigation and control solution by onboard computer is reported. Let us remind that TEAMS platform is equipped with a x86 Atom Z530 processor (1.6 GHz) and provided by the QNX real time operating system. As shown in above table, the execution time is lower than the sampling time, that is 0.1 *s* (10 Hz).

6. Conclusions

In this paper the use of SDRE technique for R&D maneuvering problem has been investigated. Particularly, the Power Series Formulation algorithm is implemented to obtain the SDRE solution. The main contribution of our research has been the validation and testing of SDRE technique on a real hardware designed to emulate on ground the proximity operations between two satellites. The experimental results have proved the feasibility of computing the solution of SDRE online on a real hardware (up to 10 Hz) also for the studied high-order system (14 variables).

7. Acknowledgment

This research was supported by the Navigation and Control Systems department of DLR – Institute of Space Systems in Bremen.

8. References

[1] J. R. Cloutier, "State-Dependent Riccati Equation Technique: An Overview," in *American Control Conference*, Albuquerque (New Messico), 1997.

[2] K. D. Hammett, "Control of Nonlinear Systems via State Feedback State-Dependent Riccati Equation Techniques," PhD Thesis, 1997.

[3] S. C. Beeler, "State-Dependent Riccati Equation Regulation of Systems with State and Control Nonlinearities," AIAA Paper 2004-3961, 2004.

[4] T. Cimen, "State-Dependent Riccati Equation (SDRE) Control: A Survey," in *17th Wold Congress The International Federetion of Automatic Control*, Seoul (Korea), 2008.

[5] G. Di Mauro, P. Di Lizia and M. Lavagna, "Control of Relative Motion via State Dependent Riccati Equation," in *AAS/IAA Astrodynamics Specialist Conference*, Anchorage (USA), 2012.

[6] E. B. Erdem and A. G. Alleyne, "Experimental Real-time SDRE Control of an Underactuated Robot," in *40th IEEE Conference on Decision and Control*, 2001.

[7] P. Dang and F. L. Lewis, "Controller for Swing-ip and Balance of Single Inverted Pendulum Using SDRE-based Solution," in *31th Annual Conference of IEEE Industrial Electronics Society*, 2005.

[8] P. K. Menon, T. Lam, L. S. Crawford and V. L. Cheng, "Real-time Computational Method for SDRE Nonlinear Control of Missiles," in *American Control Conference*, 2002.

[9] T. Cimen, "Systematic and Effective Design of Nonlinear Feedback Controllers via the State-Dependet Riccati Equation (SDRE) Method," *Annual Riview in Control,* vol. 34, no. 1, pp. 32-51, 2012.

[10] D. A. Bini, B. Iannazzo and B. Meini, Numerical Solution of Algebraic Riccati Equations, SIAM, 2012.

[11] J. A. Burghart, "A Technique for Suboptimal Feedback Control of Nonlinear System," *IEEE Tansaction on Automatic Control,* vol. 14, pp. 550-553, 1969.

[12] M. Xin and S. N. Balakrishnan, "A New Method for Suboptimal Control of a Class of Non-Linear Systems," *Optimal Control Applications and Methos,* vol. 26, pp. 55-83, 2004.

[13] M. Xin e H. Pan, «Integrated Nonlinear Optimal Control of Spacecraft in Proximity Operations,» *International Journal of Control,* vol. 83, pp. 347-363, 2009.

[14] R. H. Bartels and G. W. Stewart, "Solution of the Marix Equation AX + XB = C," *Commun ACM,* vol. 15, no. 9, pp. 820-826, 1972.

[15] J. R. Wertz, Spacecraft Attitude Determination and Control, London: Kluwer Academic Publishers, 1978.

[16] M. Schlotterer and S. Theil, "Testbed for On-orbit Servicing and Formation Dynamics Emulation," in *AIAA Guidance, Navigation, and Control Conference*, Toronto (Canada), 2010.

[17] D. Lee and H. Pernicka, "Integrated System for Autonomous Proximity Operation," *International Journal of Aeronautical & Space,* vol. 12, no. 1, pp. 43-56, 2011.

[18] D. Lee and H. Pernicka, "Optimal Control for Proximity Operations and Docking," *International Jurnal of Aeronautical and Space Science,* vol. 11, no. 3, pp. 206-220, 2006.

[19] W. Fehse, Automated, Cambridge University Press , 2003.

[20] J. R. Cloutier and D. T. Stansbery, "Control of a Continuously Stirred Tank Reactor Using an Asymmetric Solution of the State-Dependent Riccati Equation," in *International Conference of Control Applications*, Kohala Coast (Hawaii, USA), 1999.